Molecular Crystals and Liquid Crystals

Publication details, including instructions for authors and subscription information:
http://www.tandfonline.com/loi/gmcl20

Measurements of the azimuthal anchoring energy at the interface between a nematic liquid crystal and photosensitive polymers

Sandro Faetti* [a], Giorgio Mutinati [a] & Igor Gerus [b]

[a] INFM and Dipartimento di Fisica di Pisa, Pisa, Italy

[b] Institute of Bioorganic Chemistry and Petrochemistry, NASU, Kiev, Ukraine

Version of record first published: 18 Oct 2010

To cite this article: Sandro Faetti*, Giorgio Mutinati & Igor Gerus (2004): Measurements of the azimuthal anchoring energy at the interface between a nematic liquid crystal and photosensitive polymers, Molecular Crystals and Liquid Crystals, 421:1, 81-93

To link to this article: http://dx.doi.org/10.1080/15421400490501455

Mol. Cryst. Liq. Cryst., Vol. 421, pp. 81–93, 2004

ISSN: 1542-1406 print/1563-5287 online
DOI: 10.1080/15421400490501455

Taylor & Francis
Taylor & Francis Group

MEASUREMENTS OF THE AZIMUTHAL ANCHORING ENERGY AT THE INTERFACE BETWEEN A NEMATIC LIQUID CRYSTAL AND PHOTOSENSITIVE POLYMERS

Sandro Faetti and Giorgio C. Mutinati*
INFM and Dipartimento di Fisica di Pisa, via Buonarroti 2, 56127 Pisa, Italy

Igor Gerus
Institute of Bioorganic Chemistry and Petrochemistry, NASU, Kiev, Ukraine

The azimuthal anchoring energy at the interface between the nematic liquid crystal 5CB and a photosensitive polymer (para-PVCN-F) is measured using a high accuracy reflectometric method. The anchoring well is represented by the Rapini-Papoular function and the azimuthal anchoring energy coefficient W goes linearly to zero at the clearing point. Qualitative and quantitative observations show that the PVCN-F films favor a reduced surface nematic order. The gliding of the easy axis is also investigated.

pacs 61.30 Hn, 42.70.-a, 61.30 Gd, 78.20. Ci.

1. INTRODUCTION

Photosensitive polymers irradiated with polarized UV light induce an uniform alignment of nematic liquid crystals (NLCs) along an easy axis which is orthogonal to the polarization vector of the UV light [1–3]. The easy axis is characterized by the azimuthal angle ϕ_e with a x-axis in the surface plane and the pretilt angle θ_e with the surface plane. Two different mechanisms contribute to the UV induced alignment [4]: cross-linking reactions producing dimers and trans-cis transitions. The main orientational

We acknowledge the financial support by the European Community (INTAS grant 01-0170).

*Corresponding author. Tel.: 00390502214538, Fax: 0039050221433, E-mail: Faetti@df.unipi.it

properties of nematic liquid crystals at the interface with a para-PVCN-F photosensitive polymer have been already investigated [5–9].

In this paper, we use a high accuracy reflectometric method [10–12] to study the azimuthal anchoring energy, the surface nematic order and the gliding phenomena at the interface between the nematic liquid crystal 4-pentyl-4′-cyanobiphenil (5CB) and a para-PVCN-F thin layer.

2. SAMPLES PREPARATON AND EXPERIMENTAL METHOD

The 5CB nematic liquid crystal is purchased from Merk and exhibits the isotropic-anisotropic transition at the clearing temperature $T_c = 35.1^{\circ}C$. A solution of 10 μg/l of para-PVCN-F in 50% dichloroethane +50% chlorobenzene is spin coated at 3000 turns/min for 90 s on glass plates. Substrates are heated at temperature $T = 80^{\circ}C$ for 30 min. The thickness of the PVCN-F layers is about 90 nm. A linearly polarized light beam of intensity $I_o = 1.5\,mW/cm^2$ produced by high pressure mercury lamp (Osram HBO/100) impinged for 60 min on the PVCN-F film to induce an azimuthal anchoring. A not normal incidence (incidence angle $= 8^{\circ}$) was used to remove the azimuthal degeneration of the easy axes [9]. Wedge glass plates (wedge angle $\approx 1^{\circ}$) are assembled using two mylar spacers of different thickness (130 μm and 260 μm) to build a wedged cell with wedge angle $\approx 1^{\circ}$. The NLC is inserted into the cell by capillarity in the isotropic phase to avoid the anchoring memory effects produced by fluid flow [13]. A 10 mW He-Ne laser beam of wavelength $\lambda = 0.6328\,\mu m$ passes through a rotating polarizer (angular velocity $\omega = 5.7\,rad/s$) and impinges at almost normal incidence on the first glass plate of the cell. The beam reflected by the first PVCN-F-nematic interface is collected by a photodiode. Its intensity results modulated in time at the angular frequency 2ω with amplitude A and with the phase coefficient $\gamma_s = 2\phi_s + \gamma_o$, where ϕ_s represents the azimuthal angle of the director at the surface with respect a x-axis in the surface plane and γ_o is a constant. Here we set the initial easy azimuthal angle $\phi_e = 0^{\circ}$. The beam which is reflected by the first glass-air isotropic interface passes through an analyzer and is collected by an other photodiode. Then, also its intensity is modulated at the angular frequency 2ω with a reference phase coefficient γ_r which depends on the orientation of the analyzer. Using a proper orientation of the analyzer, the phase difference $\gamma = \gamma_s - \gamma_r$ can be set to $\gamma = 2\phi_s$. Amplitude A and dephasing γ are obtained from the Fourier transform of the two oscillating signals at the angular frequency 2ω. For more details on the experimental method we refer the reader to References [10–12].

3. THE PROCEDURE TO MEASURE THE AZIMUTHAL ANCHORING ENERGY

A magnetic field $\boldsymbol{H}$ oriented at an angle β with the x-axis is switched on and the consequent surface elastic torque induces a rotation of the surface director toward the magnetic field direction. According to the classical continuum theory of NLCs [14,15], the equilibrium should be reached after about six times the characteristic relaxation time $\tau_{\mathrm{r}} = \gamma_{\mathrm{r}}/(\chi_{\mathrm{a}} H^2)$, where $\gamma_{\mathrm{r}} =$ orientational bulk viscosity and $\chi_{\mathrm{a}} =$ anisotropy of the diamagnetic susceptibility (surface viscosity is always negligible). In our experimental conditions, the magnetic coherence length ξ [14] is much smaller than the local thickness d of the NLC ($d > 130\,\mu\mathrm{m}$). Then, the semi-infinite sample approximation can be used and the equilibrium of azimuthal and elastic surface torques writes:

$$\frac{\partial W(\phi_s)}{\partial \phi_s} = \sqrt{K_{22}\chi_a} H \sin(\beta - \phi_s), \tag{1}$$

where $W(\phi_{\mathrm{s}})$ is the anchoring energy function and K_{22} is the twist elastic constant of the NLC. Substituting in Eq. (1) the measured equilibrium angle ϕ_{s} together with β and with the known values of K_{22} [16] and χ_{a} [17], one can obtain the anchoring energy torque versus ϕ_{s}. Numerical integration of $\partial \mathrm{W}(\phi_{\mathrm{s}})/\partial\phi_{\mathrm{s}}$ versus ϕ_{s} leads to the anchoring energy function $W(\phi_{\mathrm{s}})$. For $\phi_{\mathrm{s}} << 1\,\mathrm{rad}$, $W(\phi_{\mathrm{s}})$ is reduced to $W(\phi_{\mathrm{s}}) = W_{\mathrm{a}}{\phi_{\mathrm{s}}}^2/2$, where W_{a} is the azimuthal anchoring energy coefficient. In this case, from Eq. (1) we get:

$$W_a = \frac{\sqrt{K_{22}\chi_a} H \sin(\beta)}{\phi_s}, \tag{2}$$

which is used to obtain the azimuthal anchoring energy coefficient.

Results (1) and (2) were obtained using the classical theory of anchoring [14,15]. However, it has been shown [18–25] that the surface azimuthal angle never reaches an equilibrium value after the switching on of a magnetic field, but a very slow drift of ϕ_{s} is observed in the experiments also for $t >> 6\ \tau_{\mathrm{r}}$. This slow drift is mainly due to a gliding of the easy axis. Points in Figure 1 show the typical dependence of $\phi_{\mathrm{s}}(t)$ on time when a magnetic field of intensity $H = 0.97\,\mathrm{kOe}$ is switched on at $t = 0$ and switched off at $t = 12.2$ hours. The full line represents the theoretical dependence which is predicted in the absence of the gliding of the easy axis (the elastic relaxation time τ_{r} is not visible with this times scale). For $t > 6\tau_{\mathrm{r}}$:

$$\phi_s(t) = \phi_s + \phi_g(t), \tag{3}$$

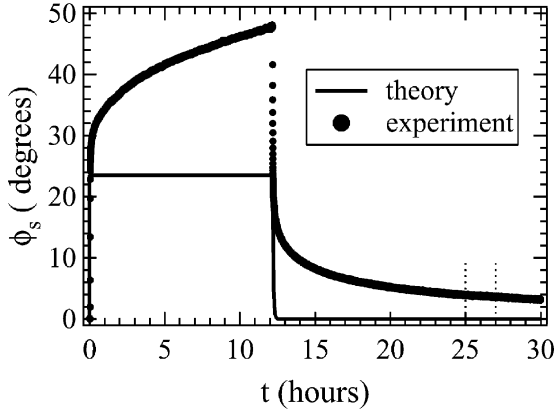

FIGURE 1 Dynamical behavior of the azimuthal director angle when a magnetic field is switched on at t = 0 and switched off at t = 12.2 hours. H = 0.97 kOe, $\beta = 80°$, $T_c - T = 1.6°C$.

where ϕ_s is the true equilibrium rotation of the director with respect to the easy axis and $\phi_g(t)$ is the slow drift of the easy axis. For $t > 6\tau_r$, $\phi_g(t)$ is represented by $\phi_g(t) = (\beta - \phi_s)\{1 - \exp[-(t/\tau)^\alpha]\}$ (the fitting curve is superimposed to points in Figure 1 for $t < 12.2$ hours). A special procedure has to be used to obtain the equilibrium rotation angle ϕ_s: the magnetic field is switched on at a given time $t = 0$ and $\phi_s(t)$ is measured; then, a best fit of the signal for times $t > 6\ \tau_r$ is made with the stretched exponential function and the true rotation ϕ_s is obtained. Then, this parameter is substituted in Eqs. (1) and (2) to obtain the anchoring energy function and the anchoring energy coefficient.

4. SURFACE ORDER AND DISTRIBUTION OF THE EASY AXES

Qualitative observations of the transition from the anisotropic phase to the isotropic phase and vice-versa with a polarizing microscope can provide informations on the surface order [26,27]. By increasing temperature T starting from the anisotropic phase, isotropic nearly planar layers nucleate at the surfaces (very small contact angle). On the contrary, by decreasing the temperature starting from the isotropic phase, the anisotropic phase nucleates as small drops (appreciable contact angles). These qualitative observations suggest that the interface induces a reduced surface nematic order [26]. Quantitative results are obtained measuring the amplitude A of the oscillating intensity. A is proportional to $\Delta R = |R_e - R_o|$ [11] where R_e and R_o are the intensity reflectivity coefficients for the extraordinary and

the ordinary polarization, respectively. $A = 0$ for a fully isotropic NLC sample, whilst $A \neq 0$ if there is a residual surface order. Figure 2a shows the temperature dependence of ΔR in the isotropic phase of 5CB versus $T - T_c$. Full points correspond to the experimental results obtained with PVCN-F, while open points represent (for comparison) the results obtained with rubbed teflon substrates that favor an excess of surface order. It is evident that $\Delta R \approx 0$ ($S_s \approx 0$). According to the Sluckin and Poniewierski theory [27], $S(z) = S_s \exp(-z/\xi_c)$ if $S_s << 1$, where z is the distance from the interface and ξ_c is the correlation length [14] ($\xi_c \approx 16\,\text{nm}$ at $T = T_c$ [28]). The local extraordinary and ordinary refractive indices of the NLC

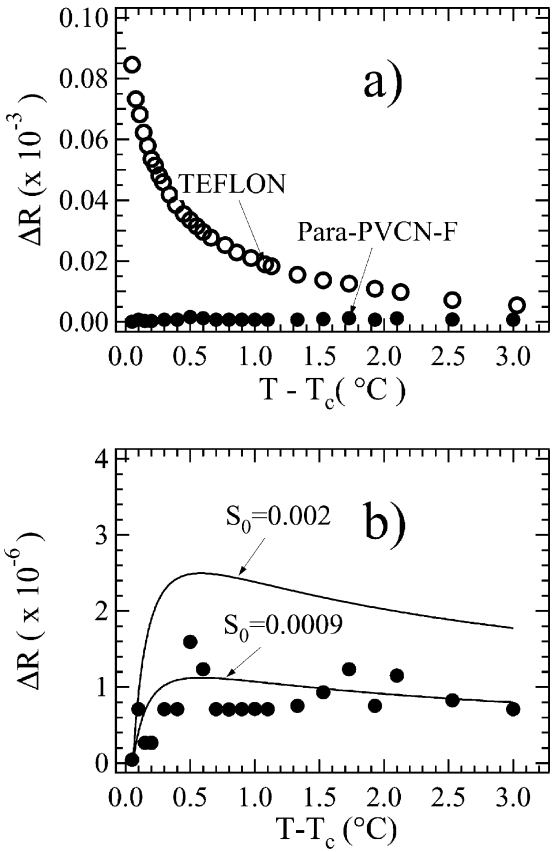

FIGURE 2 a) Temperature dependence of ΔR for the 5CB-PVCN-F interface (full points) and for a 5CB-Teflon interface (open points). b) Temperature dependence of ΔR for the 5CB-PVCN-F interface (full points) and theoretical fitting curve (bottom full line) (surface order parameter $S_s = 0.0009$).

are $n_e(z) = n_i + \eta\frac{2S(z)}{3}$ and $n_o(z) = n_i - \eta\frac{S(z)}{3}$, where n_i is the isotropic refractive index ($n_\mathrm{i} = (n_\mathrm{e} + 2n_\mathrm{o})/3$) and η is a known coefficient ($\eta = 0.376$ for 5CB [29]). Using the Born approximation for the reflection coefficients from a stratified medium ($\xi_\mathrm{c}/\lambda << 1$) [30] and disregarding the small optical anisotropy of the PVCN-F layer, we get

$$\Delta R = \frac{4\eta k_\xi S_s}{(n_i + n_p)(1 + 4k_\xi^2)}\left[\frac{k_\xi\left(\frac{\eta S_s}{3} + 2n_i - 2n_p\right)}{(n_i + n_p)} - r(2k_\xi \cos 2k_h + \sin k_h)\right], \quad (4)$$

where $r = (n_\mathrm{g} - n_\mathrm{p})/(n_\mathrm{g} + n_\mathrm{p})$ is the reflection coefficient at the glass-PVCN-F interface, $k_\xi = 2\pi n_\mathrm{i}\xi_\chi/\lambda$, $k_\mathrm{h} = 2\pi n_\mathrm{p} h/\lambda$, h is the thickness of the PVCN-F film and n_g and n_p are the refractive indices of the glass and the PVCN-F, respectively. Figure 2b shows the numerical best fit of the experimental values of ΔR with this function (lower full line) where S_s and n_p are free parameters. The other parameters are: $n_\mathrm{g} = 1.507$, $\eta = 83.5\,\mathrm{nm}$, $\lambda = 632.8$ nm, $n_\mathrm{i} = 1.583\text{–}0.00057(T - T_\mathrm{c})$ (extrapolated from [29]), $\eta = 0.376$ [29] and $\xi_\mathrm{c} = \xi_0/(T/T^\mathrm{s} - 1)^{1/2}$ where $\xi_0 = 0.66\,\mathrm{nm}$ and $T^\mathrm{s} = T_\mathrm{c} - 40\,\mathrm{mK}$ [31] (for the physical meaning of T^s we refer the reader to [31]). From the best fit we get $S_\mathrm{s} = 0.0009 \pm 0.001$ which is consistent with a null surface order parameter. The top full line represent the theoretical result obtained for $S_\mathrm{s} = 0.002$.

As shown in Reference [32], the reflectometric method provides also information about the distribution of the easy axes in the illuminated region of the surface (diameter $\approx 1\,\mathrm{mm}$). We find the Gaussian distribution

$$h(\phi_e) = \frac{1}{\sqrt{2\pi}\Delta\phi_e}\exp\left(-\frac{\phi_e^2}{2\Delta\phi_e^2}\right), \quad (5)$$

where $h(\phi_\mathrm{e})$ represents the probability of finding the local easy axis with the azimuthal angle ϕ_e and $\Delta\phi_e = 1.07^\circ \pm 0.1^\circ$ is the angular width of the distribution around a 0° average angle.

5. THE AZIMUTHAL ANCHORING ENERGY

The azimuthal anchoring energy coefficient W_a shows a small and slow continuous increase with the aging time t_a after the NLC is inserted in the cell (Fig. 3). Points in Figure 4a show the experimentally measured anchoring torque $\tau_\mathrm{s} = \partial W/\partial\phi_\mathrm{s}$ (Eq. (1) versus ϕ_s for $T - T_\mathrm{c} = 1^\circ\mathrm{C}$. Points in Figure 4b show $W(\phi_\mathrm{s})$ for three temperatures. The full lines in Figures 4a and 4b are the best fits with the Rapini-Papoular torque $\tau_s = W_a \sin(2\phi_s)/2$ and with the Rapini-Papoular function [33] $W = W_a \sin^2(\phi_s)/2$, respectively. Points in Figure 5 show the azimuthal anchoring energy coefficient W_a

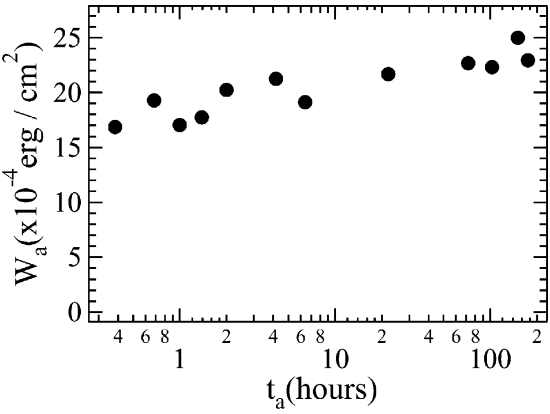

FIGURE 3 The azimuthal anchoring energy versus the aging time t_a after the introduction of the NLC in the cell. $T_c - T = 4.5\,^{\circ}C$.

(Eq. (2)) versus $T_c - T$. W_a is an increasing function of $T_c - T$ which goes to zero for $T_c - T \to 0$. The experimental results close to $T_c - T = 0^{\circ}C$ ($T_c - T < 1^{\circ}C$) are represented satisfactorily by the linear function $W_a = \alpha(T_c - T)$ (full line in Fig. 5). According to Reference [34], this theoretical dependence can be predicted using the Sluckin-Poniewierski theory [27] if the surface order approach zero for $T_c - T \to 0$ (wetting from the isotropic phase) and the surface free energy is proportional to the square power of the surface order parameter. Then, the observed temperature dependence of the anchoring energy is in agreement with the experimental observation of a small (or zero) surface order parameter at the clearing point (Fig. 2). The same kind of qualitative behavior (Figs. 2–5) was observed also for reduced UV irradiation times of the PVCN-F. The anchoring energy coefficient is an increasing function of the UV adsorbed energy in agreement with the experimental results in Reference [6].

6. THE GLIDING PHENOMENON

The drift of the surface azimuthal angle can be explained by two effects [19]: a slow decrease of W_a and a slow drift of the easy axis. This appears evident if we consider the case of small surface director rotations and small drifts of the easy axis. In this case, if W_a and ϕ_e are functions of time t, Eq. (2) becomes:

$$\varphi_s(t) = \varphi_e(t) + \frac{\sqrt{K_{22}\chi_a}H\sin(\beta)}{W_a(t)}, \tag{6}$$

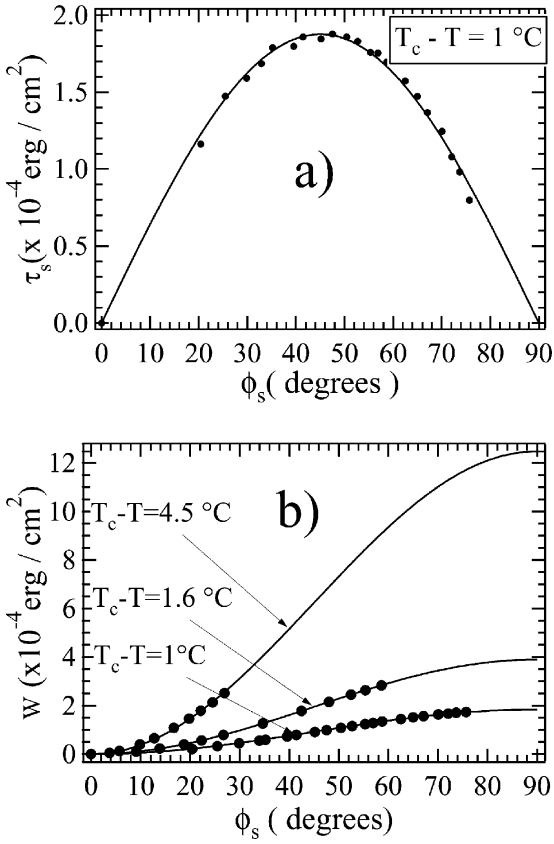

FIGURE 4 a) Surface elastic torque versus the surface azimuthal angle (points) at $T_c - T = 1°C$. To obtain the surface torque we have substituted the measured value of ϕ_s in the r.h.s. in Eq. (1) together with $\beta = 83°$ and the known values of K_{22} [16] and χ_a [17]. b) Surface azimuthal energy versus the surface azimuthal angle(points) for three different temperatures. The full lines in Figures 4a and 4b are the best fits with Rapini-Papoular torques and anchoring energies, respectively.

where $\phi_e(0) = 0$. Previous experimental results [24] showed that the slow drift of the easy axis is certainly the leading mechanism. Here we want to answer to the following question: is the anchoring energy function represented by the Rapini-Papoular function also when an appreciable gliding of the easy axis has occurred? The measurement of the Rapini-Papoular function, requires a minimum measurement time of about 2 hours. Then, the gliding of the easy axis must be negligible during the measurement time. We used the procedure below: a magnetic field was switched on at time t = 0 and switched off at time t = 12.2 hours in order to produce an

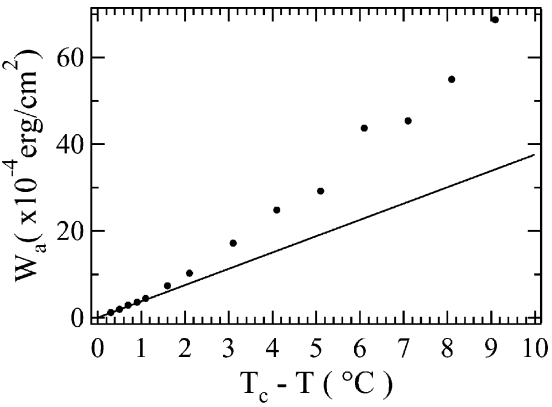

FIGURE 5 Azimuthal anchoring energy coefficient W_a versus the difference between the clearing temperature T_c and temperature T. Points (experimental results), full straight line (best fit of the results below $T_c - T = 1°C$ with the linear function $W_a = (T_c - T)$.

appreciable gliding of the easy axis. The measurement of the azimuthal anchoring torque t_s was performed in the time interval between $t =$ 25 hours to $t = 27$ hours where the easy angle is appreciably different from zero ($\phi_e \approx 7°$) but virtually constant (see Fig. 1). The corresponding experimental results are shown in Figure 6. Full points correspond to the

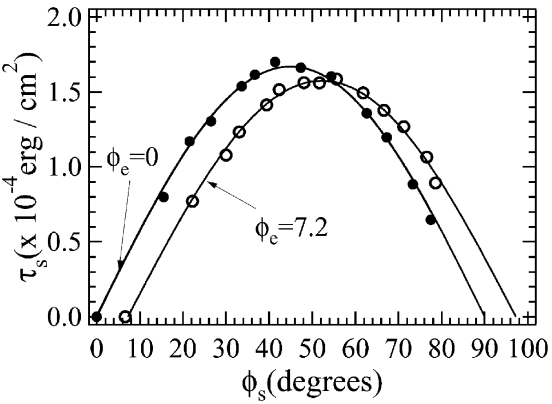

FIGURE 6 Azimuthal anchoring torque versus ϕ_s before gliding (full points) and after some gliding of the easy axis has occurred (open points). The full lines are the best fits obtained with the Rapini-Papoular torques $\tau_s = W_a \sin[2(\phi_s - \phi_e)]/2$ with $\phi_e = 0°$ and $\phi_e = 7.2°$, respectively.

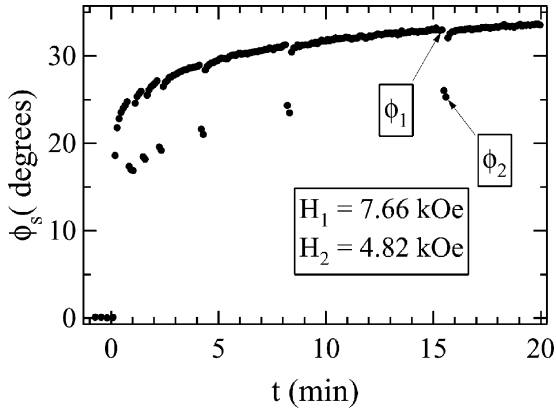

FIGURE 7 The experimental procedure used to separate the time dependences of the easy azimuthal angle and of the anchoring energy coefficient produced by the application of a magnetic torque.

experimental results obtained in the absence of gliding ($\phi_e = 0^\circ$), whilst open points represents the results obtained during the gliding ($\phi_e \approx 7^\circ$). The full lines are the best fits with two Rapini-Papoular anchoring energies centered, respectively, at $\phi_e = 0^\circ$ and $\phi_e = 7^\circ$. We infer that the Rapini-Papoular function describes the surface potential also during the gliding.

The two contributions $W_a(t)$ and $\phi_e(t)$ were obtained using the procedure below: a magnetic field $H_1 = 7.66\,\text{kOe}$ is switched on at time $t = 0$ and the corresponding surface angle $\phi_1(t)$ is measured. At given times $\bar{t}$, the magnetic field is suddendly reduced to $H_2 = 4.82\,\text{kOe}$ for a duration time of 16 s (a magnetic negative pulse) and, then, the previous field is restored (see Fig. 7). The two intensities of the magnetic field are chosen high enough so that the elastic relaxation time ($6\ \tau_r < 1\,\text{s}$) can be disregarded with respect to the gliding time. For each magnetic field pulse occurring at time $\bar{t}$, we measure the surface angles $\phi_1(\bar{t})$ and $\phi_2(\bar{t})$ immediately before and after the pulse (see Fig. 7). These angles are related to the anchoring energy trough the two equations:

$$W_a(\bar{t}) \sin\left[2\left(\phi_{1,2}(\bar{t}) - \phi_e(\bar{t})\right)\right] = 2\sqrt{K_{22}\chi_a} H_{1,2} \sin\left[\beta - \left(\phi_{1,2}(\bar{t}) - \phi_e(\bar{t})\right)\right]. \tag{7}$$

Then, substituting ϕ_1 and ϕ_2 and H_1 and H_2 in Eqs. (7) we get two nonlinear equations for the unknown parameters $\phi_e(\bar{t})$ and $W_a(\bar{t})$. The corresponding results are shown in Figures 8a and 8b.

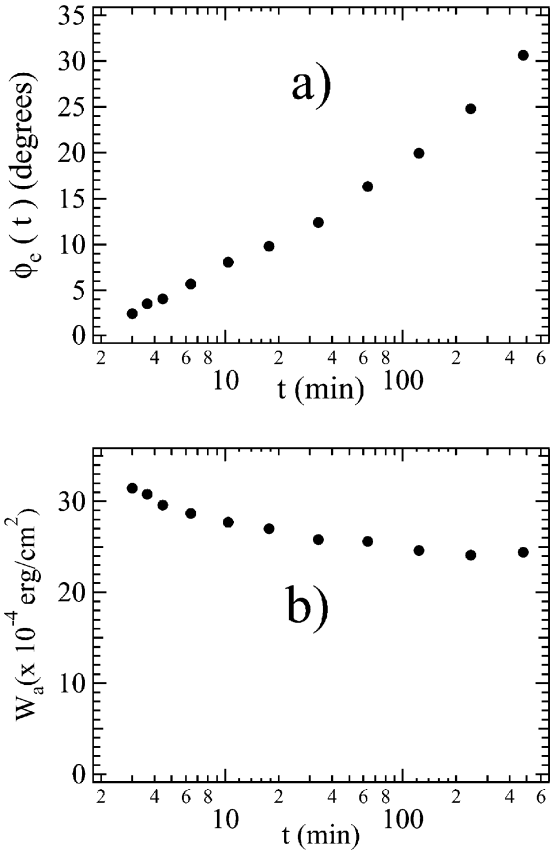

FIGURE 8 Time-dependence of ϕ_e (Fig.8a) and W_a (fig.8b) during the gliding of the easy axis.

7. CONCLUSIVE REMARKS

The azimuthal anchoring properties at the 5CB-PVCN-F interface have been investigated in detail. The local orientations of the easy axes show a Gaussian distribution with width $\Delta\phi_e \approx 1^\circ$. The surface nematic order is greatly reduced at the polymer-nematic interface. The azimuthal anchoring well is represented by the Rapini-Papoular function and the anchoring energy coefficient W_a approaches linearly zero as the temperature approaches the clearing value T_c. The azimuthal director angle shows an important drift which is described by a stretched exponential. The drift is much greater than that which is found with more conventional aligning substrates (rubbed PVA, rubbed polyimide, obliquelly evaporated SiO).

It is prevalently due to a gliding of the easy axis but also to a slow decrease of the anchoring coefficient. Such a behavior is consistent with a simple model based on anisotropic adsorption-desorption of nematic molecules at the interface [19,24].

The azimuthal anchoring energies that have been measured here are almost an order of magnitude lower than those reported for 5CB on the same substrate in ref.[6]. This difference can be explained in terms of the anisotropic adsorption of nematic molecules at the interface. In fact, in our experiment the NLC is introduced in the isotropic phase, while, in ref.[6], it was introduced in the anisotropic phase with the flow direction parallel to the easy axis. This latter procedure favors an anisotropic adsorption of nematic molecules aligned along the easy axis which leads to an increased anchoring energy [13]. These and other experimental results (very great gliding and vanishing anchoring at the clearing point) suggest strongly that an important and perhaps fundamental contribution to the azimuthal anchoring at this kind of interfaces is due to the interaction between nematic molecules adsorbed on the surface and nematic bulk molecules. Similar conclusions were reached in Reference [35] for standard PVCN substrates.

REFERENCES

[1] Dyadyusha, A., Kozerenkov, V., Marusii, T., Reznikov, Yu., Reshetnyak, V., & Khizhnayak, A. (1991). *Ukr. Fiz. Zh.*, *36*, 1059.
[2] Shadt, M., Schmitt, K., Kozenkov, V., & Chigrinov, V. (1992). *Jpn. J. Appl. Phys.*, *7*, 2155.
[3] Marusii, T. & Reznikov, Yu. (1993). *Mol. Mater.*, *3*, 161.
[4] Hichimura, K., Akita, Y., Akiyama, H., Hayashi, Y., & Kudo, K. (1996). *Jpn. J. Appl. Phys.*, *35*, L992.
[5] Adrienko, D., Dyadyusha, A., Kurioz, Yu., Reznikov, Yu., Barbet, F., Bormann, D., Warenghem, M., & Khelifa, B. (1999). *Mol. Cryst. Liq. Cryst.*, *329*, 219.
[6] Bormann, D., Kurioz, Y., Kwon, S., Reznikov, Yu., & Warenghem, M. (2000). *Liq. Cryst.*, *27*, 365.
[7] Gerus, I., Glushenko, A., Kwon, S., Reshetnyak, V., & Reznikov, Yu. (2001). *Liq. Cryst.*, *28*, 1709.
[8] Bugayova, L., Gerus, I., Glushenko, A., Dyadyusha, A., Kuriov, Yu., Reshetnyak, V., Reznikov, Yu., & West, J. (2002). *Liq. Cryst.*, *29*, 209.
[9] Hashimoto, T., Sagiyama, T., Katoh, K., Saitch, T., Suzuki, H., Limura, Y., & Kobayashi, S. (May 1990). *Poceedings of the SID Digest of Technical Papers*, 877.
[10] Faetti, S., Palleschi, V., & Schirone, A. (1988). *Il Nuovo Cimento 10D*, 1313.
[11] Faetti, S. & Nobili, M. (1998). *Liq. Cryst.*, *25*, 487.
[12] Faetti, S. & Mutinati, G. C. (2003). *Eur. Phys. J. E*, *10*, 265.
[13] Yokoyama, H., Kobayashi, S., & Kamei, H. (1984). *J. Appl. Phys.*, *56*, 2645.
[14] de Gennes, P. G. (1974). *The physics of liquid crystals*, Clarendon: Oxford.
[15] Faetti, S. (1991). *Physics of Liquid Crystalline Materials*, Khoo, I. C. & Simoni, F. (Eds.), Gordon and Breach Science Publishers.
[16] Toyooka, T., chen, G., Takezoe, H., & Fukuda, A. (1987). *Jpn. J. Appl. Phys.*, *26*, 1959.

[17] Scherrel, P. L. & Crellin, D. A. (1979). *J. Phys. Colloq.*, *40*, C3-213.
[18] Faetti, S., Nobili, M., & Schirone, A. (1991). *Liq. Cryst.*, *10*, 95.
[19] Raggi, I. (1993). Thesis University of Pisa.
[20] Nose, T., Masuda, S., & Sato, S. (1991). *Jpn. J. Appl. Phys.*, *30*, 3450.
[21] Sato, Y., Sato, K., & Uschida, T. (1992). *Jpn. J. Appl. Phys.*, *31*, L579.
[22] Vorflusev, V. P., Kitzerow, H. S., & Chigrinov, V. G. (1997). *Appl. Phys. Lett.*, *70*, 3359.
[23] Barberi, R., Dozov, I., Giocondo, M., Iovane, M., Martinot-Lagarde, P., Stoenescu, D., Tonchev, S., & Tsonev, L. V. (1998). *Eur. Phys. J. B.*, *6*, 83.
[24] Faetti, S., Nobili, M., & Raggi, I. (1999). *Eur. Phys. J. B*, *11*, 445.
[25] Stoenescu, D., Dozov, I., & Martinot-Lagarde, P. (2000). *Mol. Cryst. Liq. Cryst.*, *351*, 427.
[26] Yokoyama, H., Kobayashi, S., & Kamei, H. (1992). *Appl. Phys. Lett.*, *41*, 438.
[27] Sluckin, T. J. & Poniewierski, A. (1985). In: *Fluid Interfacial Phenomena*, (Eds.), Croxton, C. A. John Wiley.
[28] Coles, H. J. & Stratielle, C. (1979). *Mol. Cryst. Liq. Cryst.*, *55*, 273.
[29] Karat, P. & Madhusudana, N. V. (1976). *Mol. Cryst. Liq. Cryst.*, *36*, 51.
[30] Wu, E. S. & Webb, W. W. (1973). *Phys. Rev. A 8*, 2065.
[31] Hsiung, H., Rasing, Th., & Shen, Y. R. (1986). *Phys. Rev. Lett.*, *57*, 3065.
[32] Campanelli, E., Faetti, S., & Nobili, M. In press on *Eur. Phys. J. E 11*.
[33] Rapini, A. & Papoular, M., (1969). *J. Phys. Colloq. France 30*, C4–54.
[34] Faetti, S., Gatti, M., Palleschi, V., & Sluckin, T. J. (1985). *Phys. Rev. Lett.*, *55*, 1681.
[35] Klopcar, N., Drevensek-Olenik, I., Copic, M., Kim, M. W., Rastegar, A., & Rasing, Th. (2003). *Mol. Cryst. Liq. Cryst.*, *368*, 395.